Thermal Emission Modulation by Electron Population in Quantum Dots

Yu Gu,* Haixiao Xu, and Zhi Li†
Key Laboratory of Advanced Display Materials and Devices, Ministry of Industry and Information Technology, College of Material Science and Engineering, Nanjing University of Science and Technology, Nanjing, 210094 China

(Received 13 July 2023; revised 31 August 2023; accepted 20 April 2024; published 21 May 2024)

We report an efficient temperature modulation of thermal emissivity near room temperature using quantum dots. The quantum confinement effects result in a unique feature that resembles a quasi-two-level electronic system (QTLES). The QTLES's dielectric function $\varepsilon(\omega)$ is shown to be dependent on the electron population difference $\delta\rho(T)$, which exhibits strong temperature dependence and can be tuned by adjusting the Fermi-level of the solid. Experiments with the Ag_2Se quantum dots confirm the theory and showcase a modulate rate $d\epsilon/dT \approx 1.5 \times 10^{-3}$ K^{-1} that meets the requirements for engineering applications. This study demonstrates an exciting new avenue for temperature modulation of thermal emission and may open up new possibilities for applications like energy harvesting, thermal camouflage, thermal rectifications, and many others.

DOI: 10.1103/PhysRevLett.132.216901

All physical systems with temperature greater than 0 K spontaneously emit electromagnetic radiations into the environment. The two fundamental laws governing this process are Planck's law [1] and Kirchhoff's law [2,3]. The former characterizes the far field spectral radiance $I_{bb}(\omega, T)$ of a blackbody at temperature T. The latter states that the spectral emissivity ϵ_ω (the spectral radiance ratio between a real object and a blackbody) and the absorptivity α_ω (determined by material's dielectric function and geometry) are equal in the objects satisfying time-reversal symmetry. Under these two laws, the emission spectrum of a real object follows the general form $\epsilon_\omega I_{bb}(\omega, T) = \alpha_\omega I_{bb}(\omega, T)$. It has enabled the photonic engineering to reshape the emission spectrum on demand [4–6] and found great successes for applications including energy harvesting [7–10], thermal management [11–14], radiative cooling [15–18], infrared imaging [19], thermophotovoltaics [20,21], etc.

In the majority of the aforementioned studies, the spectral emissivity ϵ_ω is typically assumed to be temperature independent. The temperature dependence of thermal emission arises solely from the Bose-Einstein distribution of photons. This assumption is generally valid, particularly in the vicinity of room temperature, leading to the Stefan-Boltzmann law for a spectrum-integrated total emission proportional to T^4. Modifying the Stefan-Boltzmann temperature exponent requires identifying materials with temperature-dependent spectral emissivity $\epsilon_\omega(T)$. This approach enables a more flexible temperature dependence in total emission, unlocking a wide range of potential applications including self-adapting thermal management [22–24], thermal camouflage [25–28], high resolution thermograph [29], thermal rectifications [30–33], etc. Unfortunately, at present, the predominant option for achieving substantial temperature modulation of ϵ_ω is limited to vanadium dioxide (VO_2) due to its special metal-insulator transition near 340 K [34]. The Ge-Sb-Te alloys represent another, less explored option that relies on the amorphous-to-crystal phase transitions [35]. In both cases, the electronic states of the system experience noticeable changes and the dynamic range of temperature modulation confines to the proximity of the transition temperature, significantly limiting the choice of materials.

Achieving strong temperature-dependent spectral emissivity $\epsilon_\omega(T)$ without substantially varying the electronic states still remains to be a great challenge. This letter demonstrates an efficient temperature modulation of emissivity via electron population in Ag_2Se quantum dots (QDs). We derive the temperature dependent dielectric function of a quasi-two-level electronic system (QTLES) based on quantum kinetic equations. The large tunablity of thermal emissivity arises from the Fermi-Dirac statistics [see Fig. 1(a)] with the Fermi level playing a crucial role. Experiments with Ag_2Se QDs validate the theory, demonstrating strong temperature modulation of emissivity with the same orders of magnitude as that for VO_2. The proposed system does not require a significant change of electronic states. In principle, it is applicable to a wide range of semiconductor QDs if the similar QTLES appears. We believe that the proposed mechanism offers new opportunities for advancing the field and exploring more potential applications.

The phenomenology of a two-level system was investigated in Ref. [36], where the dielectric function of the following form:

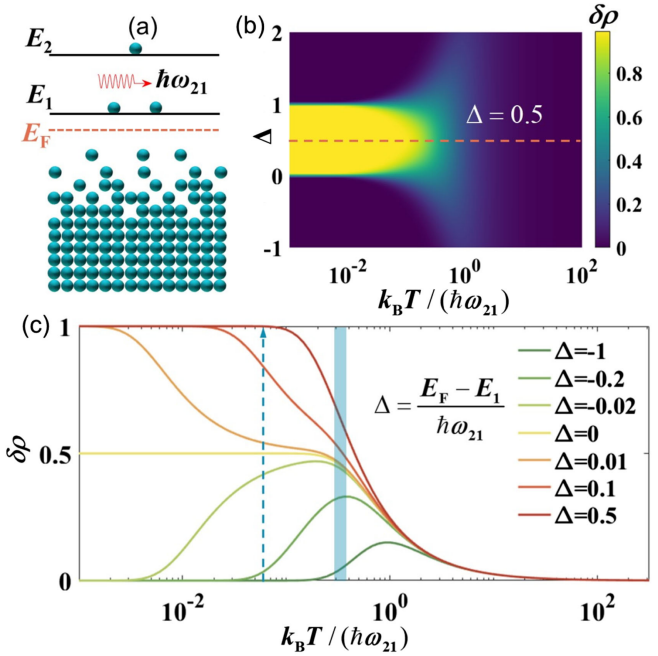

FIG. 1. (a) Schematic illustration of a quasi-two-level electronic system. (b) Population difference $\delta\rho$ as a function of temperature and the position of the Fermi level. (c) Illustration of $\delta\rho$ as a function of temperature for several different values of Δ. $\Delta = (E_F - E_1)/\hbar\omega_{21}$ characterizes position of the Fermi level. Shaded region corresponds to the near room temperature range of 273 to 373 K for $\hbar\omega_{21} = 0.124$ eV.

$$\varepsilon(\omega) = \varepsilon_\infty + \delta\rho(T)\frac{\Omega\omega_{21}}{\omega^2 - \omega_{21}^2 - 2i\omega\gamma} \tag{1}$$

was proposed. Equation (1) resembles a classical Lorentzian oscillator [37] with an additional factor $\delta\rho(T)$ standing for the temperature-dependent electron population difference. The other parameters are the same as those for a Lorentzian oscillator: ε_∞ is the high frequency permittivity, ω_{21} is the resonant frequency relating the two energy levels E_1 and E_2 as $E_2 - E_1 = \hbar\omega_{21}$[Fig. 1(a)], Ω is the oscillator strength, and γ is the damping frequency. The phenomenological theory of Ref. [36] does not allow us to find the functional form of $\delta\rho(T)$ and it was postulated to follow the Gibb's distribution. Surprisingly, a notable absence exists in explicitly treating a two-level system with quantum mechanics, which would yield the classical Lorentzian oscillator in Eq. (1). Investigations into photonic interactions with electronic levels, such as quantum dots, typically focus on absorption and emission rates under Fermi's golden rule [38–40]. To establish a robust quantum mechanical framework and derive the accurate functional form of $\delta\rho$, we solve the quantum kinetic equation for electrons interacting with light in solids (Supplemental Material [41]):

$$\frac{\partial\rho}{\partial t} = \frac{1}{i\hbar}[H,\rho] + \gamma(\rho - \rho^{(0)}), \tag{2}$$

where ρ is the density operator characterizing the probability of a single electron occupying different electronic states in the system. Equation (2) is a quantum analog of the Boltzmann transport equation [44,45]. The single electron Hamiltonian $H = H^{(0)} + H^{(1)}$ is divided into two parts: $H^{(0)}$, the original Hamiltonian, and $H^{(1)}$, a perturbation due to photon-electron interactions. Equation (2) also includes a term for electron scattering and relaxation, characterized by the damping frequency γ. This term ensures the electron system returns to equilibrium with the distribution function $\rho^{(0)}$. As $H^{(1)}$ is small compared to $H^{(0)}$, i.e., $H^{(1)} \ll H^{(0)}$, the change in ρ is also small, i.e., $\rho = \rho^{(0)} + \rho^{(1)}$ with $\rho^{(1)} \ll \rho^{(0)}$. This small change $\rho^{(1)}$ determines the dipole moment induced by the light.

The original electronic eigenstates $|n\rangle$, i.e., $H^{(0)}|n\rangle = E_n|n\rangle$ of the system are assumed to be known and are taken as the basis for the representation in Eq. (2). The operator $\rho^{(0)}$ is diagonal and it resembles the Fermi-Dirac distribution under thermal equilibrium:

$$\rho_{nn}^{(0)} = \langle n|\rho^{(0)}|n\rangle = \frac{2}{N}\frac{1}{\exp\left(\frac{E_n - E_F}{k_BT}\right) + 1}. \tag{3}$$

k_B is the Boltzmann constant, N is the total number of electrons in the system, factor 2 accounts for the spin degeneracy and E_F is the Fermi energy. It becomes clear that the temperature T naturally appears in the fundamental Eq. (2), thereby will have a profound impact on the optical property and emissivity of the material.

With a weak perturbation ($H^{(1)} \ll H^{(0)}$ and $\rho^{(1)} \ll \rho^{(0)}$), Eq. (2) is expanded to first order using perturbation theory (see Supplemental Material [41]):

$$\frac{\partial}{\partial t}\rho_{nm}^{(1)} = -(i\omega_{nm} + \gamma)\rho_{nm}^{(1)} - i\frac{H_{nm}^{(1)}}{\hbar}\left(\rho_{mm}^{(0)} - \rho_{nn}^{(0)}\right). \tag{4}$$

The first order approximation is sufficiently accurate in majority of the light-matter interaction problems (Supplemental Material [41]). The frequency ω_{nm} follows $\hbar\omega_{nm} = E_n - E_m$. All the other terms with subscripts m, n are matrix elements, i.e., $Q_{mn} = \langle m|Q|n\rangle$. Equation (4) can be readily solved if the term $H_{nm}^{(1)}$ is specified. We define the perturbation term $H^{(1)}$ as $-ez\xi_0\cos\omega t$, representing an interaction with electromagnetic wave polarized in the z direction. ξ_0 is the amplitude, ω is the angular frequency, z is the electron's position operator, and $p = -ez$ is the dipole moment operator (e: the elementary charge). $H_{nm}^{(1)} = -z_{nm}e\xi_0\cos\omega t$ with $z_{nm} = \langle n|z|m\rangle$ can be estimated with the known wave functions of the eigenstates. By solving Eq. (4), $\rho_{nm}^{(1)}$ can be found and the expectation value of the induced dipole moment is calculated as (see Supplemental Material [41]):

$$\langle p\rangle = \sum_n \langle n|\rho^{(1)} p|n\rangle = \frac{e^2}{\hbar}\sum_{m,n}|z_{mn}|^2(\rho^{(0)}_{mm}-\rho^{(0)}_{nn})\mathrm{Re}\left(\frac{\omega_{nm}}{\omega^2-\omega^2_{nm}-2i\omega\gamma}\xi_0 e^{i\omega t}\right). \quad (5)$$

The average dipole moment per electron, $\langle p\rangle$, determines the electric polarization ($N\langle p\rangle/V$, where V is the volume). The complex dielectric function $\varepsilon(\omega)$ is then calculated with the fundamental constitutive relation [46], i.e., $\varepsilon_0\mathrm{Re}([\varepsilon(\omega)-1]\xi_0 e^{i\omega t}) = N\langle p\rangle/V$ (ε_0: permittivity of vacuum). Only energy levels satisfying $\omega_{nm}=\omega$ will interact resonantly with photons of energy $\hbar\omega$. In this case, $m=1$, $n=2$ with the constraint that $E_2 > E_1$. Nonresonant contributions ($\omega_{nm}\neq\omega$) are grouped into a frequency-independent constant ε_∞, which may also include other contributions such as ionic polarization. In this way, Eq. (1) can be recovered, with $\delta\rho$ and Ω defined as

$$\delta\rho = \frac{N}{2}\left(\rho^{(0)}_{11}-\rho^{(0)}_{22}\right) = \frac{1}{\exp\left(\frac{E_1-E_F}{k_BT}\right)+1} - \frac{1}{\exp\left(\frac{\hbar\omega_{21}}{k_BT}\right)\exp\left(\frac{E_1-E_F}{k_BT}\right)+1}, \quad (6)$$

$$\Omega = \frac{2e^2|z_{12}|^2}{V\hbar\varepsilon_0}. \quad (7)$$

$\delta\rho$ offers a direct mean to manipulate the optical property of QTLES by adjusting the temperature and is the central term to achieve strong temperature dependent emissivity $\epsilon_\omega(T)$.

The temperature dependence of $\delta\rho$ is shown in Fig. 1(b). The dimensionless parameter $\Delta = (E_F - E_1)/\hbar\omega_{21}$ denotes the position of the Fermi level. It becomes obvious that $\delta\rho$ is symmetric with respect to $\Delta = 0.5$, i.e., placing Fermi levels at Δ and $1-\Delta$ yield the exact same temperature dependence. Figure 1(c) is a clearer illustration of the temperature dependence of $\delta\rho$ when the position of the Fermi level is varied. In the high temperature limit, $\delta\rho$ decays to zero in all cases corresponding to a flattening of the Fermi-Dirac distribution. The case for $\Delta < 0$ is of great interest as the population difference $\delta\rho$ exhibits a nonmonotonic dependence on temperature and reaches maximum at some particular temperature. It is a unique feature of the proposed QTLES as compared to the two-level media phenomenologically proposed by Baranov [36] which only shows monotonously decreasing behavior of $\delta\rho$. It stems from the "quasi" nature of our two-level system. In contrast to a strictly two-level system as proposed in Ref. [36], the presence of the Fermi level in our model indicates that electrons are distributed across all electronic states within the system, rather than being confined to the two specific levels associated with thermal emission. This feature allows for both increasing and decreasing spectral emissivity with the temperature within the same system, offering notable potential for temperature modulations.

The shaded region corresponds to the room temperature range (273–373 K) for $\hbar\omega_{21}\approx 0.124$ eV and $\mathrm{d}\delta\rho/\mathrm{d}T$ can be either positive or negative in this range depending on the position of the Fermi level. On the other hand, as indicated by the dashed arrow line in Fig. 1(c), $\delta\rho$ varies from 0 to 1 by tuning the position of the Fermi level. This adjustment can be achieved via doping during the fabrication process or with postfabrication *in situ* electrostatic gating, a standard technique widely used for field effect transistors, i.e., a complete turning on and off of the thermal radiation may be realized if an external basis voltage is applied.

Figure 2(a) shows the imaginary part of the dielectric function $\mathrm{Im}[\varepsilon(\omega)]$ at different temperatures. It is a key factor determining the absorptivity or emissivity of the QTLES. The simulation parameters are $\varepsilon_\infty = 4$, $\hbar\omega_{21}\approx 0.124$ eV, $\Delta = -0.9$, $\Omega = 1.5\omega_{21}$, $\gamma = 0.4\omega_{21}$. The value of $\hbar\omega_{21}$ matches 10 μm peak emission wavelength near room temperature. Δ is negative to demonstrate a positive $\mathrm{d}\delta\rho/\mathrm{d}T$. $\varepsilon_\infty = 4$ is a typical value for inorganic materials. The value of Ω is estimated with Eq. (7) by setting $z_{12}\sim 10^{-10}$ m (typical atomic distance), $V\sim 10^{-27}$ m^3 (typical size of a quantum dot). It gives $\hbar\Omega\sim 0.1$ eV (comparable to $\hbar\omega_{21}$). $\hbar\gamma$ is assumed to have

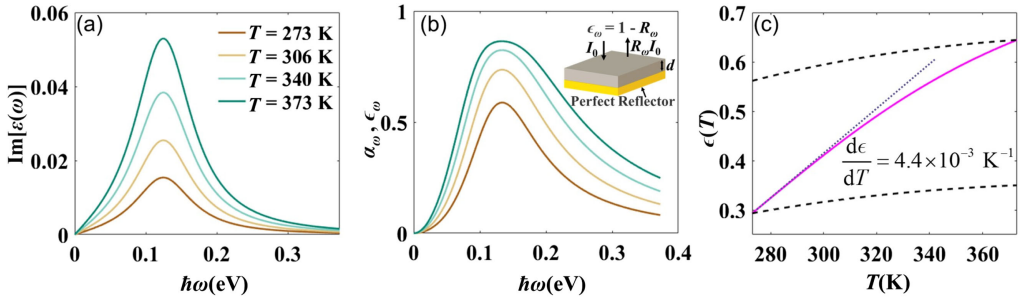

FIG. 2. (a) Temperature dependent imaginary part of the dielectric function of a QTLES. (b) Spectral emissivity at different temperatures of a 100 μm thick film coated on a perfect infrared reflector. (c) The spectrum integrated total emissivity as a function of temperature.

a similar order to $k_B T$, which at 300 K is approximately 0.01 eV or $\sim 0.1\hbar\omega_{21}$. The imaginary part shown in Fig. 2(a) gradually increases with temperature indicating a stronger absorptivity or emissivity as temperature rises. Even though the imaginary part appears to be small, the emissivity of the film may become large if the QTLES is sufficiently thick. According to the Kirchhoff's law, the spectral emissivity of a homogeneous film of QTLES coated on a perfect reflector [inset of Fig. 2(b)] can be calculated with the ray tracing method [47] (see Supplemental Material [41]).

$$\epsilon_\omega = \alpha_\omega = 1 - \frac{R_0 + (1-2R_0)\exp(-\tilde{d})}{1 - R_0\exp(-\tilde{d})},$$
$$\tilde{d} = 8\pi\frac{d}{\lambda}\mathrm{Im}\left[\sqrt{\varepsilon(\omega)}\right]. \tag{8}$$

$R_0 = |(n-1)/(n+1)|^2$ ($n = \varepsilon^{1/2}$ is the refractive index) is the interfacial reflectance at the QTLES and vacuum interface, λ is the wavelength of light in vacuum, and d is the film thickness. The spectral absorptivity or emissivity is mainly controlled by the dimensionless length $\tilde{d}$. Figure 2(b) illustrates the temperature-dependent spectral emissivity ϵ_ω for a film made of QTLES with thickness $d = 100$ μm. An obvious increase of ϵ_ω can be observed with the increasing temperature in the range of 273–373 K. The spectrum-integrated total emissivity $\epsilon(T)$ can be further calculated as

$$\epsilon(T) = \frac{\int_0^\infty \epsilon_\omega(T) I_{bb}(\omega,T)\mathrm{d}\omega}{\int_0^\infty I_{bb}(\omega,T)\mathrm{d}\omega},$$
$$I_{bb}(\omega,T) = \frac{\hbar\omega^3}{4\pi^3 c^2}\frac{1}{\exp\left(\frac{\hbar\omega}{k_B T}\right) - 1}. \tag{9}$$

c is the speed of light. A strong temperature dependency of $\epsilon(T)$ is evident as indicated by the solid line in Fig. 2(c). The maximum value of $\mathrm{d}\epsilon/\mathrm{d}T$ reaches 4.4×10^{-3} K^{-1} which has the same order of magnitude as VO_2 [25]. As explained in Refs. [25,48], achieving a $\mathrm{d}\epsilon/\mathrm{d}T$ value of at least 10^{-3} K^{-1} is crucial for practical applications and the proposed QTLES easily satisfy this requirement. This pronounced temperature modulation stems directly from the temperature-dependent spectral emissivity ϵ_ω [Fig. 2(b)]. Importantly, it is not due to the frequency dispersion of ϵ_ω, which only creates a weak temperature dependence $\mathrm{d}\epsilon/\mathrm{d}T \sim 10^{-4}$ K^{-1} [two dashed lines in Fig. 2(c)]. These lines are constructed by substituting the function $\epsilon_\omega(T)$ with its value at two fixed temperatures, i.e., 273 and 373 K, respectively, in Eq. (9).

Experimentally realizing such a QTLES in bulk crystal is challenging since electronic states are typically continuous. Semiconductor quantum dots (QDs) offer a solution through quantum confinement effects, creating discrete states near the band edge as size decreases. Experimental works [43,49,50] already reported resonant light absorptions near 10 μm in infrared QDs. The absorption is attributed to the intraband transition between the $1S_e$ to $1P_e$ level [50–52] in the conduction band. We followed the method reported by Ref. [53] to synthesize colloidal Ag_2Se QDs with an average diameter of 6.2 nm (Supplemental Material [41]). The QD dispersion was deposited on an ITO substrate (IR reflector) and its reflectance was measured after solvent evaporation. Temperature control was achieved with a controller attached to the substrate (details in Supplemental Material [41]). By experimentally measuring the reflectance of the bare ITO substrate (R_{ITO}) and that of the QD-coated sample (R_{QD}), we obtained the experimental spectral emissivity ϵ_ω as $1 - R_{\mathrm{QD}}/R_{\mathrm{ITO}}$. It corresponds to the spectral emissivity of an ensemble of QDs on a perfect reflector (see Supplemental Material [41]). Equation (8) remains applicable with $R_0 = 0$ for a relatively sparse dispersion of QDs. By setting $R_0 = 0$, the spectral emissivity becomes

$$\epsilon_\omega = 1 - \exp(-\tilde{d}), \qquad \tilde{d} = 6\chi\frac{\omega}{c}d\,\mathrm{Im}\left[\frac{\varepsilon(\omega)-1}{\varepsilon(\omega)+2}\right]. \tag{10}$$

The dimensionless thickness $\tilde{d}$ depends on the QD's absorption cross section [54] and volume fraction χ (see Supplemental Material [41]). Since the imaginary part of $\varepsilon(\omega)$ is typically small [Fig. 2(a)], with the help of Eq. (1), one may expand the dimensionless thickness $\tilde{d}$ to the first order as

$$\tilde{d} \approx \beta\delta\rho\,\mathrm{Im}\left(\frac{\omega\omega_{21}}{\omega^2 - \omega_{21}^2 - 2i\omega\gamma}\right), \quad \beta = \frac{6\chi\Omega d}{c(\varepsilon_\infty + 2)^2}. \tag{11}$$

Equations (6) and (11) indicate that only four unknowns, namely β, $\Delta = (E_F - E_1)/\hbar\omega_{21}$, ω_{21}, γ are needed to determine the spectral emissivity described by Eq. (10). These four unknowns were adjusted to fit the experimental spectral emissivity. The dimensionless β reflects the combined contributions from oscillator strength (Ω), QD's concentration (χ), and film thickness (d). The theoretical spectral emissivity at different temperatures agree fairly well with the experimental data [Figs. 3(a) and 3(b)]. The fitting parameters are $\beta = 3.43 \pm 0.04$, $\Delta = -0.190 \pm 0.002$, $\hbar\omega_{21} = (204.4 \pm 0.2)$ meV, $\hbar\gamma = (107.6 \pm 0.6)$ meV. All the parameters are rounded up to the first uncertain digit. Sharp peaks appearing in the experimental data originate from the ligands attached to the QD's surface [53,55]. Apart from the contribution from ligand groups, the imperfect fitting between the experimental data and theory may arise from polydispersity (a distribution over ω_{21}, γ, and Ω among quantum dots of different sizes) and a possibly temperature-dependent γ (Supplemental Material [41]).

Even though the fitting is not perfect, the observed trend shows a clear increase in ϵ_ω with rising temperatures.

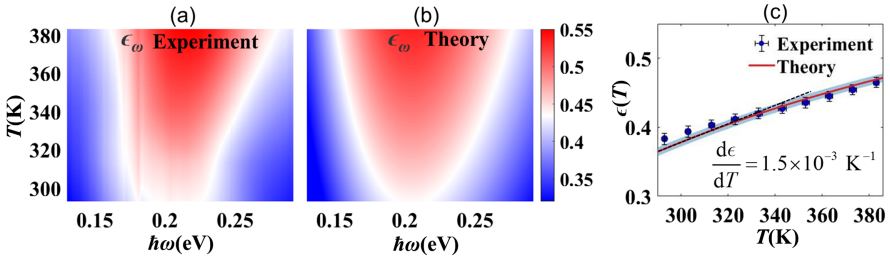

FIG. 3. (a) Experimental spectral emissivity of a thin layer dispersion of Ag_2Se QDs at different temperatures. (b) Theoretical fitted spectral emissivity at different temperatures. (c) The spectrum integrated total emissivity as a function of temperature. Shaded area shows the 97% confidence interval. The error bars are generated based on the data shown in Supplemental Material [41].

As previously discussed, this is a unique feature of QTLES and is attributed to the gradual increase of population difference $\delta\rho$ for a negative Δ which is consistent with the fitting result $\Delta = -0.190$. Meanwhile, a nice agreement is achieved for the integrated emissivity as shown by Fig. 3(c). The temperature modulation rate $d\epsilon/dT$ reaches 1.5×10^{-3} K^{-1} which is much greater than that of a temperature independent Lorentzian oscillator [dashed lines in Fig. 2(c)] and also surpass the 10^{-3} K^{-1} requirement for practical applications. Moreover, experiments with QDs of smaller size (~3.7 nm) exhibit a negative modulation rate (see Fig. S11 in Supplemental Material [41]). According to Fig. 2, a negative modulation rate in the room temperature range suggests a near-zero or positive Δ indicating that the relative position of Fermi level varies with particle size. Further investigations into the detailed electronic structure and an accurate determination of the total number of electrons are necessary to clarify the evolution of Δ and the temperature modulation rate with particle size. The current experiment serves as a proof of concept, and we anticipate improved temperature modulation with further optimization and fine-tuning of the system. An order of magnitude estimation suggests the possibility of achieving a modulation rate of $\sim 1 \times 10^{-2}$ K^{-1} (Supplemental Material [41]) with the proposed QTLES, surpassing the highest value $\sim 8 \times 10^{-3}$ K^{-1} with VO_2 [25]. Meanwhile, this strategy may extend to higher frequencies (visible or near-infrared) by varying energy difference ($\hbar\omega_{21}$) and Fermi level position. If $(E_F - E_1) \sim k_B T$ [Fig. 1(c)], a strong temperature dependence can still be achieved near room temperature. For practical implementations, the position of the Fermi level is tuned by injecting or withdrawing electrons from the quantum dots, a potentially challenging task due to the impediment of electron transport by surface ligands.

In conclusion, our study showcases a quasi-two-level electronic system for achieving efficient thermal emission modulation near room temperature. By exploiting the electron population difference between the two electronic levels, we have effectively regulated the optical properties of materials via temperatures, with the position of the Fermi level serving as the key controlling factor. Theoretical analysis predicts a unique nonmonotonic behavior and a promising modulation rate ($d\epsilon/dT$) of 4.4×10^{-3} K^{-1}, highlighting its potential as a versatile method for emissivity control. A proof-of-concept experiment with Ag_2Se QDs shows relatively good agreement with theoretical predictions, achieving a temperature modulation rate of 1.5×10^{-3} K^{-1}. We believe that the proposed QTELS may open up exciting avenues for further exploration and advancement in the field of dynamic modulation of thermal emissions.

The authors are grateful for fruitful discussions with Professor Konstantin G. Kornev from Clemson University. This work was supported by the Natural Science Foundation of Jiangsu Province (BK 20200071).

*Corresponding author: yug@njust.edu.cn
†Corresponding author: zhili@njust.edu.cn

[1] M. Planck, *The Theory of Heat Radiation* (Blakiston, New York, 1914).
[2] S. Chandrasekhar, *Radiative Transfer* (Courier Corporation, New York, 2013).
[3] G. B. Rybicki and A. P. Lightman, *Radiative Processes in Astrophysics* (John Wiley & Sons, New York, 1991).
[4] X. Liu, T. Tyler, T. Starr, A. F. Starr, N. M. Jokerst, and W. J. Padilla, Phys. Rev. Lett. **107**, 045901 (2011).
[5] D. G. Baranov, Y. Xiao, I. A. Nechepurenko, A. Krasnok, A. Alù, and M. A. Kats, Nat. Mater. **18**, 920 (2019).
[6] R. Hu, W. Xi, Y. Liu, K. Tang, J. Song, X. Luo, J. Wu, and C.-W. Qiu, Mater. Today **45**, 120 (2021).
[7] W. Li, S. Buddhiraju, and S. Fan, Light Sci. Appl. **9**, 68 (2020).
[8] Z. Wu, J. Wang, Y. Liu, S. Hou, X. Liu, Q. Zhang, and F. Cao, Mater. Today Phys. **18**, 100388 (2021).
[9] S. Buddhiraju, W. Li, and S. Fan, Phys. Rev. Lett. **124**, 077402 (2020).
[10] T. A. Cooper, S. H. Zandavi, G. W. Ni, Y. Tsurimaki, Y. Huang, S. V. Boriskina, and G. Chen, Nat. Commun. **9**, 5086 (2018).
[11] P.-C. Hsu *et al.*, Sci. Adv. **3**, e1700895 (2017).
[12] P.-C. Hsu, A. Y. Song, P. B. Catrysse, C. Liu, Y. Peng, J. Xie, S. Fan, and Y. Cui, Science **353**, 1019 (2016).
[13] J. K. Tong, X. Huang, S. V. Boriskina, J. Loomis, Y. Xu, and G. Chen, ACS Photonics **2**, 769 (2015).

[14] J. D. Hardy and E. F. DuBois, Proc. Natl. Acad. Sci. U.S.A. **23**, 624 (1937).
[15] A. P. Raman, M. A. Anoma, L. Zhu, E. Rephaeli, and S. Fan, Nature (London) **515**, 540 (2014).
[16] N. N. Shi, C.-C. Tsai, F. Camino, G. D. Bernard, N. Yu, and R. Wehner, Science **349**, 298 (2015).
[17] J. N. Munday, Joule **3**, 2057 (2019).
[18] L. Zhou, J. Rada, Y. Tian, Y. Han, Z. Lai, M. F. McCabe, and Q. Gan, Phys. Rev. Mater. **6**, 090201 (2022).
[19] X. Tang, M. M. Ackerman, M. Chen, and P. Guyot-Sionnest, Nat. Photonics **13**, 277 (2019).
[20] O. Ilic, P. Bermel, G. Chen, J. D. Joannopoulos, I. Celanovic, and M. Soljačić, Nat. Nanotechnol. **11**, 320 (2016).
[21] A. LaPotin *et al.*, Nature (London) **604**, 287 (2022).
[22] K. Tang *et al.*, Science **374**, 1504 (2021).
[23] S. Wang, T. Jiang, Y. Meng, R. Yang, G. Tan, and Y. Long, Science **374**, 1501 (2021).
[24] Y. Cui *et al.*, Joule **2**, 1707 (2018).
[25] K. Tang *et al.*, Adv. Mater. **32**, 1907071 (2020).
[26] A. Shahsafi *et al.*, Proc. Natl. Acad. Sci. U.S.A. **116**, 26402 (2019).
[27] M. A. Kats, R. Blanchard, S. Zhang, P. Genevet, C. Ko, S. Ramanathan, and F. Capasso, Phys. Rev. X **3**, 041004 (2013).
[28] Y. Qu, Q. Li, L. Cai, M. Pan, P. Ghosh, K. Du, and M. Qiu, Light Sci. Appl. **7**, 26 (2018).
[29] K. Tang, K. Dong, C. J. Nicolai, Y. Li, J. Li, S. Lou, C.-W. Qiu, D. H. Raulet, J. Yao, and J. Wu, Sci. Adv. **6**, eabd8688 (2020).
[30] Q. Li, Q. Chen, and B. Song, Mater. Today Phys. **23**, 100632 (2022).
[31] C. R. Otey, W. T. Lau, and S. Fan, Phys. Rev. Lett. **104**, 154301 (2010).
[32] P. Ben-Abdallah and S.-A. Biehs, Appl. Phys. Lett. **103**, 191907 (2013).
[33] Q. Li, H. He, Q. Chen, and B. Song, Phys. Rev. Appl. **16**, 014069 (2021).
[34] M. F. Picardi, K. N. Nimje, and G. T. Papadakis, J. Appl. Phys. **133**, 111101 (2023).
[35] K.-K. Du, Q. Li, Y.-B. Lyu, J.-C. Ding, Y. Lu, Z.-Y. Cheng, and M. Qiu, Light Sci. Appl. **6**, e16194 (2017).
[36] I. A. Nechepurenko and D. G. Baranov, Opt. Lett. **46**, 3584 (2021).
[37] H. A. Lorentz, *The Theory of Electrons and Its Applications to the Phenomena of Light and Radiant Heat* (GE Stechert & Company, New York, 1916), Vol. 29.
[38] P. A. M. Dirac and N. H. D. Bohr, Proc. R. Soc. A **114**, 243 (1927).
[39] V. I. Klimov, A. A. Mikhailovsky, S. Xu, A. Malko, J. A. Hollingsworth, C. A. Leatherdale, H.-J. Eisler, and M. G. Bawendi, Science **290**, 314 (2000).
[40] S. Franke, J. Ren, M. Richter, A. Knorr, and S. Hughes, Phys. Rev. Lett. **127**, 013602 (2021).
[41] See Supplemental Material at http://link.aps.org/supplemental/10.1103/PhysRevLett.132.216901 for detailed derivations of the dielectric constant, the emissivity of a thin film as well as experimental details and error analysis, which includes Refs. [42,43].
[42] G. A. F. Seber and C. J. Wild, *Nonlinear Regression*, Wiley Series in Probability and Statistics (Wiley-Interscience, Hoboken, NJ, 2003).
[43] M. R. Scimeca, N. Mattu, I. J. Paredes, M. N. Tran, S. J. Paul, E. S. Aydil, and A. Sahu, J. Phys. Chem. C **125**, 17556 (2021).
[44] C. L. Tang, *Fundamentals of Quantum Mechanics: For Solid State Electronics and Optics* (Cambridge University Press, Cambridge, England, 2005).
[45] S. Harris, *An Introduction to the Theory of the Boltzmann Equation* (Courier Corporation, New York, 2004).
[46] J. D. Jackson, *Classical Electrodynamics*, 3rd ed. (Wiley, New York, 1999).
[47] Z. M. Zhang, *Nano/Microscale Heat Transfer* (McGraw-Hill, New York, 2007).
[48] D. M. Bierman, A. Lenert, M. A. Kats, Y. Zhou, S. Zhang, M. De La Ossa, S. Ramanathan, F. Capasso, and E. N. Wang, Phys. Rev. Appl. **10**, 021001(R) (2018).
[49] E. Lhuillier, M. Scarafagio, P. Hease, B. Nadal, H. Aubin, X. Z. Xu, N. Lequeux, G. Patriarche, S. Ithurria, and B. Dubertret, Nano Lett. **16**, 1282 (2016).
[50] S. E. Keuleyan, P. Guyot-Sionnest, C. Delerue, and G. Allan, ACS Nano **8**, 8676 (2014).
[51] M. Park, D. Choi, Y. Choi, H.-b. Shin, and K. S. Jeong, ACS Photonics **5**, 1907 (2018).
[52] J. Son, D. Choi, M. Park, J. Kim, and K. S. Jeong, Nano Lett. **20**, 4985 (2020).
[53] A. Sahu, A. Khare, D. D. Deng, and D. J. Norris, Chem. Commun. (Cambridge) **48**, 5458 (2012).
[54] C. F. Bohren and D. R. Huffman, *Absorption and Scattering of Light by Small Particles* (Wiley, New York, 1983).
[55] A. Heuer-Jungemann *et al.*, Chem. Rev. **119**, 4819 (2019).